Critical Care

RESEARCH

Open Access

# Alteration in early resting-state functional MRI activity in comatose survivors of cardiac arrest: a prospective cohort study

Rui Shao[1†], Tao Wang[1†], Chenchen Hang[1], Le An[1], Xingsheng Wang[1], Luying Zhang[1], Jingfei Yu[1], Zhenyu Shan[1], Qi Yang[2*] and Ziren Tang[1*]

## Abstract

**Background** This study aimed to explore the characteristics of abnormal regional resting-state functional magnetic resonance imaging (rs-fMRI) activity in comatose patients in the early period after cardiac arrest (CA), and to investigate their relationships with neurological outcomes. We also explored the correlations between jugular venous oxygen saturation (SjvO2) and rs-fMRI activity in resuscitated comatose patients. We also examined the relationship between the amplitude of the N20-baseline and the rs-fMRI activity within the intracranial conduction pathway of somatosensory evoked potentials (SSEPs).

**Methods** Between January 2021 and January 2024, eligible post-resuscitated patients were screened to undergo fMRI examination. The amplitude of low-frequency fluctuation (ALFF), fractional ALFF (fALFF), and regional homogeneity (ReHo) of rs-fMRI blood oxygenation level-dependent (BOLD) signals were used to characterize regional neural activity. Neurological outcomes were evaluated using the Glasgow–Pittsburgh cerebral performance category (CPC) scale at 3 months after CA.

**Results** In total, 20 healthy controls and 31 post-resuscitated patients were enrolled in this study. The rs-fMRI activity of resuscitated patients revealed complex changes, characterized by increased activity in some local brain regions and reduced activity in others compared to healthy controls ($P < 0.05$). However, the mean ALFF values of the whole brain were significantly greater in CA patients ($P = 0.011$). Among the clusters of abnormal rs-fMRI activity, the cluster values of ALFF in the left middle temporal gyrus and inferior temporal gyrus and the cluster values of ReHo in the right precentral gyrus, superior frontal gyrus and middle frontal gyrus were strongly correlated with the CPC score ($P < 0.001$). There was a strong correlation between the mean ALFF and SjvO2 in CA patients ($r = 0.910$, $P < 0.001$). The SSEP N20-baseline amplitudes in CA patients were negatively correlated with thalamic rs-fMRI activity (all $P < 0.001$).

**Conclusions** This study revealed that abnormal rs-fMRI BOLD signals in resuscitated patients showed complex changes, characterized by increased activity in some local brain regions and reduced activity in others. Abnormal BOLD signals were associated with neurological outcomes in resuscitated patients. The mean ALFF values

[†]Rui Shao and Tao Wang contributed equally to this work.

*Correspondence:
Qi Yang
yangyangqiqi@gmail.com
Ziren Tang
tangziren1970@163.com
Full list of author information is available at the end of the article

of the whole brain were closely related to SjvO2 levels, and changes in the thalamic BOLD signals correlated with the N20-baseline amplitudes of SSEP responses.

**Trial registration** NCT05966389 (Registered July 27, 2023).

**Keywords** Cardiac arrest, Rs-fMRI, BOLD signal, Prognosis, SjvO2, SSEP

## Background

In comatose patients resuscitated from cardiac arrest (CA), hypoxic ischemic brain injury (HIBI) is a prominent factor contributing to mortality and long-term disability [1, 2]. A challenge in the clinical management of HIBI patients is that patients with similar clinical manifestations may have markedly different outcomes, ranging from complete recovery, and mild cognitive deficits to minimal consciousness states, or even death [3]. Reliable early prediction of neurological outcomes in resuscitated patients is important for the development of appropriate therapeutic protocols. Current post-resuscitation guidelines recommend a multimodal approach for predicting adverse outcomes, including clinical examination, electrophysiology, serum biomarkers, and neuroimaging [4]. However, these metrics are able to reliably predict outcomes for only approximately 30–50% of CA survivors [5, 6]. Therefore, there is an urgent need in clinical practice to improve the capability of early prognostic assessment for patients after CA.

Resting-state functional magnetic resonance imaging (rs-fMRI) is a non-invasive imaging technique based on blood oxygen level-dependent (BOLD), signals that operate on the principle of detecting relative concentration changes in oxyhemoglobin and deoxyhemoglobin [7]. The rs-fMRI BOLD signal is characterized by its high spatial resolution, and sensitivity to both cortical and subcortical neuronal activities [8]. Detailed characterization of the alterations in brain activity after HIBI can be achieved with rs-fMRI BOLD signals. Previous rs-fMRI studies have demonstrated that cerebral functional network connectivity, especially default-mode network (DMN), was associated with neurological outcomes [8–10]. These studies showed that the disruption of DMN connectivity was predictive of poor outcome in CA survivors. However, most of these studies did not quantify abnormal neural activity in specific brain regions, enrolled homogeneous patient populations, or clarified the confounding factors that may affect BOLD signals. Furthermore, the timing of MRI examinations after CA varied widely. Due to the varying tolerances of different brain regions to ischemia and hypoxia, we hypothesized that early changes in regional or global BOLD signals may correlate with the neurological outcomes of CA survivors.

Jugular venous oxygen saturation (SjvO2) reflects the disparity between the oxygen entering the brain and the oxygen consumed by brain tissue [11]. Previous studies have shown that increased mean SjvO2 is associated with unfavorable outcomes in patients following CA [12, 13]. While rs-fMRI activity relies on the relative levels of oxyhemoglobin and deoxyhemoglobin. We hypothesized that there may be a correlation between SjvO2 and the mean whole-brain rs-fMRI activity in comatose patients after resuscitation. Somatosensory evoked potential (SSEP) recordings after CA provide valuable information for the prediction of neurological outcomes [4]. The intracerebral conduction pathways for SSEP include the thalamus, insula, the posterior bank of the central sulcus, the postcentral gyrus at the omega zone, and other regions [14, 15]. Some studies have suggested that the N20-baseline amplitude of SSEP is correlated with neurologic outcomes in CA survivors [16, 17]. The N20-baseline amplitude may depend on the extent of damage to the intracranial conduction pathway. We hypothesized that N20-baseline amplitude may be correlated with rs-fMRI activity within the intracranial conduction pathway of SSEP.

Given the above considerations, we explored the characteristics of abnormal regional rs-fMRI BOLD signals in comatose patients in the early period after CA, ensuring the homogeneity of the enrolled patient population and the consistency of potential confounding factors. Furthermore, we investigated their relationships with neurological outcomes. Additionally, we explored the correlations between SjvO2 and BOLD signals in resuscitated comatose patients. We also examined the relationship between the N20-baseline amplitude and BOLD signals within the intracranial conduction pathway of SSEP.

## Methods

### Study design and participants

This study is a post hoc analysis of rs-fMRI BOLD signals in post-resuscitated patients. Between January 2021 and January 2024, we consecutively screened post-resuscitated patients admitted to the emergency intensive care unit (EICU) after out of hospital cardiac arrest (OHCA) with a presumed cardiac cause, of the witnesses. All patients were unconscious and unable to obey verbal commands. The exclusion criteria were: patients younger

than 18 years of age, patients with unwitnessed asystole, patients with comborbid brain injury (stroke, cerebral haemorrhage, etc.), patients who were pregnant, patients with MRI contraindications such as extracorporeal membrane oxygenation (ECMO) or pacemakers, patients with haemoglobin less than 120 g/L, and patients whose family members did not agree to the study.

Post-resuscitated patients were transferred to the EICU for further standardized management in accordance with guidelines. All the patients received temperature control to maintain a target temperature of 33 °C for 24 h using Arctic Sun® (Arctic Sun® 5000, BD, USA) feedback-controlled surface cooling device. Then, the temperature of the patients was gradually increased to 37 °C with a rewarming rate of 0.1 °C/h. Patients received mechanical ventilation and were sedated, primarily with propofol and remifentanil. The sedation protocol was based on the Richmond Agitation–Sedation Scale (RASS) and was titrated to obtain a RASS of − 5. Other treatment protocols were provided according to the international guidelines for post-cardiac arrest care. A jugular vein balloon catheter was inserted in all patients. The catheter was inserted retrograde into the jugular innervating vein identified by ultrasound. When there was no difference in the jugular vein diameter between the two sides, the right side was preferred. Ultimately, correct placement of the catheter tip (with the tip located above the inferior border of the C1 vertebra) was confirmed by lateral cervical radiography. SSEP recordings were performed using a Neuron Spectrum-5 (Neurosoft, Russia). SSEP was measured after stimulation of the right and left median nerves using bipolar surface electrodes at the wrist. The following data were extracted from the prospective registry: age, sex, years of education, vascular risk factors. Bystander cardiopulmonary resuscitation (CPR) and time from CPR to return of spontaneous circulation (ROSC).

After successful rewarming and maintenance of normothermia, and haemodynamic stability for 24 h, resuscitated patients underwent MRI (Siemens 3 Tesla Prisma MRI system, Germany), specifically blood oxygenation level dependent functional magnetic resonance imaging (BOLD-fMRI). The rs-fMRI BOLD signals were acquired using an EPI sequence with the following parameters: repetition time = 1000 ms, echo time = 30 ms, flip angle = 70°, field of view = 220 mm × 220 mm, bandwidth = 1820 Hz/pixel, 60 axial slices, slice thickness = 2 mm, the final voxel size = 2 mm × 2 mm × 2 mm, with 300 volumes. During the examination, the supervising physician accompanied the patient to maintain the patient's RASS at − 5 and monitored the patient's vital signs using a magnetic resonance monitoring system (Siemens Healthcare Prism, Germany). Patients who were on ventilators were mechanically ventilated using a magnetic ventilator (HAMILTON-MRI, USA). SjvO2, haemoglobin and arterial blood gas (ABG) testing, and the serum neuron specific enolase (NSE) concentration were measured within 1 h after fMRI. SSEP was recorded in patients after fMRI and 48 h after the discontinuation of sedation. The N20-baseline amplitude between the N20 peak and baseline in the left cerebral hemisphere was measured. The neurological outcomes were evaluated using the Glasgow–Pittsburgh Cerebral Performance Category (CPC) scale at 3 months after ROSC. The CPC score ranges from 1 to 5, with 1 indicating good performance, 2 indicating moderate disability, 3 indicating severe disability, 4 indicating vegetative state and 5 indicating brain death or death. The neurological outcomes were categorized as favorable prognosis (CPC 1–2) and poor prognosis (CPC 3–5). This study was approved by the Beijing Chao-yang Hospital Ethics Committee (No. 2023-ke-406). Written informed consent was obtained from all patients and/or legal surrogates.

#### fMRI data preprocessing and analysis

The amplitude of low-frequency fluctuations (ALFF), fractional ALFF (fALFF), and regional homogeneity (ReHo) were employed to quantify spontaneous activity in brain regions and the synchronicity of neuronal activity within local brain areas [18, 19]. ALFF and fALFF can be utilized for the detection of local spontaneous brain activity [7]. ReHo assesses the coherence of fMRI signal time courses between a voxel and its neighboring voxels, typically indicating the synchronization of neuronal activity within local brain regions [7]. FMRI data preprocessing was conducted using the Data Processing Assistant for rs-fMRI Advanced Edition (DPARSF) software (The Mathworks, Inc., Natick, MA, USA, available at http://rfmri.org/content/dparsf), which is based on MATLAB 2016b (Mathworks Inc.). FMRI data preprocessing and analysis were performed by professionals who were blinded to the clinical data. Preprocessing involved removing the first 20 time-point fMRI images, applying slice-timing correction using the middle slice as a reference, and spatially realigning all volumes to correct for head movements. Head motion was evaluated and corrected via rigid body registration, excluding subject exceeding the maximum translation of 2.0 mm or rotation of 2.0 degrees. Spatial normalization of the realigned volumes to the Montreal Neurological Institute space was performed using an EPI template, resampling images to a voxel size of 3 mm × 3 mm × 3 mm. Nuisance covariates (24 motion parameters, their first derivations, white matter, and cerebrospinal fluid) were regressed out, and the effects of low-frequency drift and high-frequency physiological noise were minimized through time band-pass filtering (0.01–0.10 Hz).

DPARSF software was also used for ALFF, fALFF and ReHo analysis. To obtain the power spectrum, voxel time series were transformed into the frequency domain using fast Fourier transformation. The power spectrum was then square-rooted and averaged over the 0.01–0.10 Hz range for each voxel, defining the ALFF. The fALFF represents the ratio of the sum of amplitudes in the 0.01–0.10 Hz range over the entire frequency spectrum. The standardized ALFF/fALFF values of each voxel were obtained by normalization to the global mean ALFF/fALFF values. Subsequently, a Gaussian kernel of 6 mm FWHM was applied for smoothing. ReHo was calculated for each voxel using Kendall's coefficient of concordance (KCC), assessing the temporal similarity with its 26 nearest voxels. The standardized ReHo was derived by normalizing each voxel's KCC against the whole brain's mean KCC, followed by smoothing with a 6 mm FWHM Gaussian kernel.

### Statistical analysis

Categorical variables are described as frequencies with percentiles. Continuous variables were described as median values with interquartile ranges (IQRs). Categorical variables were compared between groups using the $\chi 2$ test corrected for continuity in a $2\times2$ table or Fisher exact test. Continuous variables were compared using Student's t test or the Mann–Whitney U test, as appropriate. To assess the between-group differences in ALFF, fALFF, and ReHo between healthy controls and CA patients, a two-sample t test was performed, with age, sex, and years of education as covariates, using the Statistical Parametric Mapping software package (SPM12) in MATLAB 2016b. Brain regions were reported based on an uncorrected voxel-wise height threshold of $P<0.001$ combined with an FWE-corrected cluster-wise threshold of $P<0.05$ for multiple comparison correction. Receiver operating characteristic (ROC) curves were constructed to assess the prognostic performance in predicting poor neurological outcomes at 3 months. The correlation of measurement data was assessed by Spearman or Pearson analysis. All the statistical tests were two-tailed, and a $P$ value less than 0.05 was considered to indicate statistical significance. Statistical analyses were performed using SPSS version 26.0 software (IBM, Chicago, IL, USA) and GraphPad Prism 10 (GraphPad, La Jolla, CA).

## Results

### Patient characteristics

In total, a cohort of 132 comatose patients with OHCA that was presumed to have a cardiac cause were screened. Of these patients, 24 patients had unwitnessed asystole, 47 patients had hemodynamic instability, 8 patients had a previous history of brain disease, 6 patients had contraindications for MRI, 3 patients had a hemoglobin concentration less than 120 g/L, 4 patients refused to be enrolled, 3 patients had significant artefacts on MRI due to obvious head motion, and 6 patients lost to follow-up. Thus, 31 patients were ultimately included in the study (Fig. 1). Notably, 90-days after ROSC, 12 (39%) and 19 (61%) patients were assigned to the CPC 1–2 and CPC 3–5 groups, respectively. And 8 (CPC = 5) of these patients died. Moreover, 20 healthy right-handed volunteers were recruited for the control group. The baseline characteristics of the patients are shown in Table 1. There were no significant differences between the groups regarding age, sex, years of education or vascular risk factors. The median time from CA to ROSC in the CPC 3–5 group was greater than that in the CPC 1–2 group (25 min vs. 17 min, $P=0.010$). The median value of SjvO2, serum NSE, SSEP responses, and the left N20-baseline amplitude were significantly different between the two groups.

### Characteristics of rs-fMRI BOLD signals in cardiac arrest patients

ALFF method was conducted to measure the activity of different brain regions in CA patients (Table 2 and Additional file 1: Table S1). The mean ALFF values of the whole brain were significantly greater in CA patients than in healthy controls ($P=0.010$). Moreover, ALFF values were elevated in some brain regions but decreased in others (Fig. 1). Compared with healthy controls, the ALFF values in the bilateral precuneus cortex of post-resuscitated patients were significantly lower, with a total cluster size of 387 voxels ($P<0.001$, Fig. 2A). However, increased ALFF values were observed in the bilateral paracentral lobule, the postcentral gyrus, median cingulate, and white matter of the right frontal, parietal, and insula lobes, with a total cluster size of 948 voxels ($P<0.001$, Fig. 2B, C). Compared to the CPC 3–5 group, the CPC 1–2 group had significantly elevated ALFF values in the left middle temporal gyrus cortex and inferior temporal gyrus cortex, with a cluster size of 330 voxels ($P=0.002$, Fig. 2D).

The fALFF values were also measured in different subgroups (Table 2 and Additional file 1: Table S1). Whole-brain mean fALFF values in CA patients were not significantly different from those in healthy controls ($P=0.057$). However, the fALFF values of the cortical regions in the bilateral superior parietal gyrus, bilateral occipital lobes, left cerebellum, and right temporal lobe were significantly lower in CA patients than in healthy controls (all $P<0.05$, Fig. 2E).

There were also significant differences in the ReHo values between groups (Table 2 and Additional file 1: Table S1). Compared with healthy controls, the ReHo

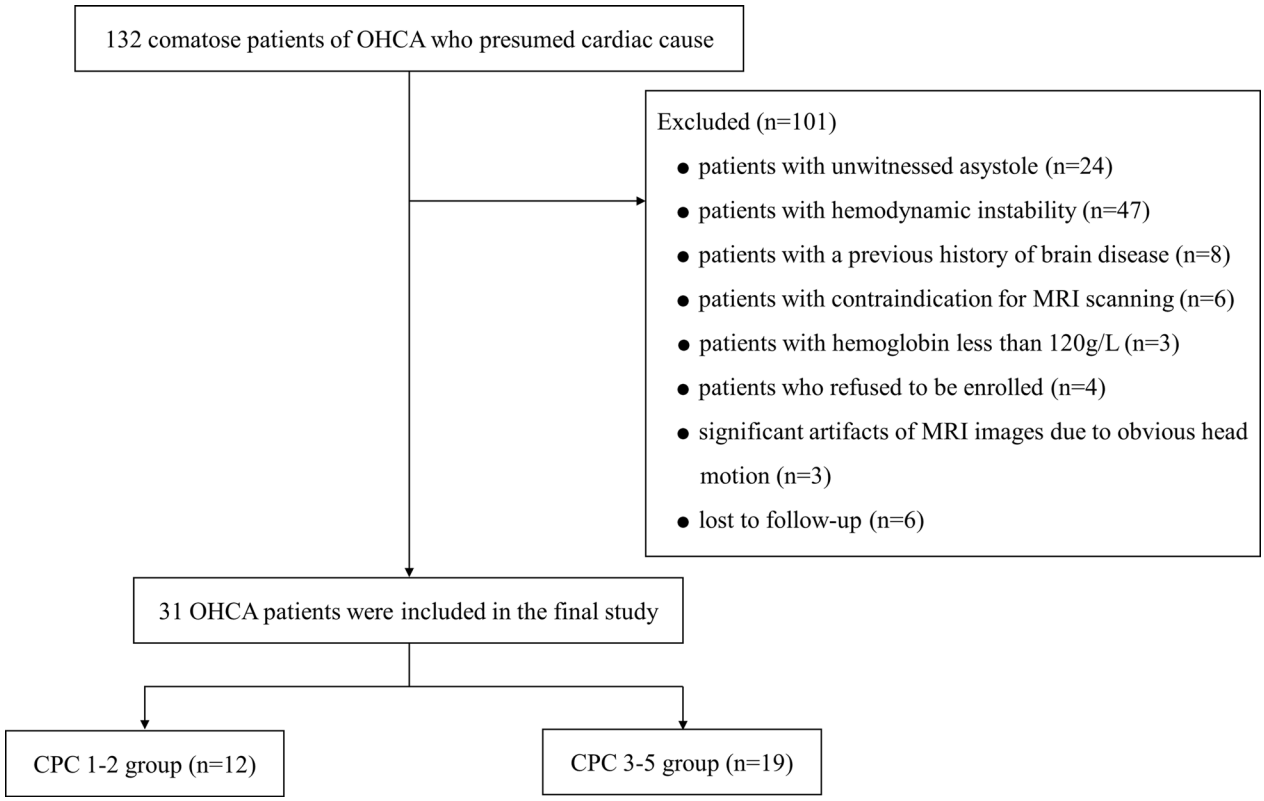


**Fig. 1** Flow diagram of patients based on CONSORT

values in the bilateral frontal and parietal lobes, occipital lobe, and median and posterior cingulate gyrus were decreased in CA patients, with a total cluster size of 2732 voxels (all $P < 0.001$, Fig. 2F). However, the CA patients had significantly increased ReHo values in the bilateral fusiform gyrus, hippocampus, parahippocampus, insula, cerebellum (4–5), vermis (1–5), right putamen, and white matter of bilateral temporal lobe, with a total cluster size of 7784 voxels, with the majority of these voxels located in the subcortex ($P = 0.002$, Fig. 2G). Compared with the CPC 3–5 group, the CPC 1–2 group showed elevated ReHo values of the cortical regions in the right precentral gyrus, superior frontal gyrus, middle frontal gyrus, and bilateral parietal lobe, with a cluster size of 330 voxels ($P < 0.001$, Fig. 2H). However, significantly decreased ReHo values in the subcortical regions were observed, significant reductions were noted in the left insula, left hippocampus, parahippocampal region, and the white matter of the left frontal and temporal lobes in the CPC 1–2 group compared to the CPC 3–5 group (all $P < 0.01$, Fig. 2I).

#### Predictive potential of rs-fMRI BOLD signals: ROC curve analysis

ROC curves were established to evaluate the predictive qualities of the rs-fMRI BOLD signals (Additional file 2: Table S2). Among the clusters with abnormal ALFF values, the maximum area under the curve (AUC) for predicting prognosis of CPC 3–5 was found in the cluster of the left middle temporal gyrus and inferior temporal gyrus, with an AUC of 0.794 ($P = 0.007$, Fig. 3 red line). Among the clusters with abnormal fALFF values, the cluster of the left superior parietal gyrus had the highest AUC for predicting prognosis of CPC 3–5, with a value of 0.728 ($P = 0.035$, Fig. 3 yellow line). The maximum AUC of the ReHo values for predicting prognosis of CPC 3–5 was observed in the cluster of the right precentral gyrus, superior frontal gyrus, and middle frontal gyrus, with an AUC of 0.943 ($P < 0.001$, Fig. 3 blue line). Interestingly, the AUC of the serum NSE concentration for predicting prognosis of CPC 3–5 was 0.820 ($P = 0.003$, Fig. 3 green line).

**Table 1** Baseline demographic data and arrest characteristics

| Variables | Healthy controls | CA patients | *P* value | CA patients | | *P* value |
|---|---|---|---|---|---|---|
| | | | | CPC 1–2 | CPC 3–5 | |
| Number | 20 | 31 | – | 12 | 19 | – |
| Age, y | 56 (52–59) | 55 (46–62) | 0.668 | 55 (43–59) | 59 (46–65) | 0.978 |
| Male, n (%) | 12 (60.0%) | 20 (64.5%) | 0.745 | 8 (64.3%) | 12 (60.0%) | 1.000 |
| Education, y | 12 (12–16) | 12 (12–16) | 1.000 | 12 (12–16) | 12 (12–16) | 0.834 |
| DM, n (%) | 6 (30.0%) | 10 (29.4%) | 0.865 | 3 (25.0%) | 7 (36.8%) | 0.697 |
| Hypertension, n (%) | 6 (30.0%) | 14 (44.1%) | 0.279 | 5 (41.7%) | 9 (47.4%) | 1.000 |
| Dyslipidaemia, n (%) | 5 (25.0%) | 7 (20.6%) | 0.842 | 2 (16.7%) | 5 (26.3%) | 0.676 |
| Smoking | 7 (35.0%) | 12 (35.3%) | 0.789 | 4 (33.3%) | 8 (42.1%) | 0.717 |
| Alcohol consumption | 5 (25.0%) | 13 (38.2%) | 0.217 | 5 (41.7%) | 8 (42.1%) | 1.000 |
| Bystander CPR | – | 16 (50.0%) | – | 7 (58.3%) | 9 (47.4%) | 0.716 |
| Time to ROSC, min | – | 20 (16–26) | – | 17 (13–20) | 25 (17–30) | 0.010 |
| pH | – | 7.37 (7.35–7.42) | – | 7.37 (7.36–7.40) | 7.38 (7.35–7.42) | 0.679 |
| PaO2 (mmHg) | – | 104 (93–114) | – | 107 (97–120) | 101 (93–113) | 0.223 |
| PaCO2 (mmHg) | – | 40 (37–42) | – | 38 (36–41) | 40 (37–43) | 0.279 |
| Haemoglobin (g/L) | 133 (126–138) | 128 (124–134) | 0.219 | 130 (123–135) | 127 (124–134) | 0.500 |
| SjvO2 (%) | – | 77 (69–84) | – | 69 (63–76) | 83 (75–88) | < 0.001 |
| Serum NSE (ng/mL) | 5.8 (3.8–8.4) | 56.8 (39.5–93.7) | < 0.001 | 40.8 (29.2–65.9) | 86.4 (47.5–101.2) | 0.006 |
| SSEP responses, n (%): | | – | | | 0.018 | |
| Bilaterally absent | – | 6 (19.3%) | | 0 | 6 (31.6%) | |
| Unilaterally present | – | 3 (9.7%) | | 0 | 3 (15.8%) | |
| Bilaterally present | – | 22 (71.0%) | | 12 (100%) | 10 (52.6%) | |
| Left N20-baseline amplitude (μV) - | 0.68 (0–1.28) | – | 1.38 (1.18–1.66) | 0.38 (0–0.62) | < 0.001 | |

Data are shown as median and interquartile range unless otherwise indicated

CA cardiac arrest, CPC cerebral performance category, CPR Cardiopulmonary resuscitation, DM Diabetes mellitus, NSE neuron specific enolase, PaCO2 Partial pressure of carbon dioxide in arterial blood, PaO2 Partial pressure of oxygen in arterial blood, ROSC return of spontaneous circulation, SjvO2 Jugular venous oxygen saturation, SSEP Somatosensory evoked potentials

#### Correlations between rs-fMRI BOLD signals and CPC scores

Correlation analyses were performed between the rs-fMRI BOLD signals and CPC scores in CA patients. Among the clusters with abnormal ALFF values, the best correlation was found in the cluster of the left middle temporal gyrus and inferior temporal gyrus, which showed negative correlation with the CPC score ($r = -0.630$, $P < 0.001$, Fig. 4A). Abnormal fALFF values of all the clusters had poor correlations with CPC scores ($P > 0.05$). However, among the clusters with abnormal ReHo values, the cluster values of the right precentral gyrus, superior frontal gyrus and middle frontal gyrus showed a strong negative correlation with CPC scores ($r = -0.812$, $P < 0.001$, Fig. 4B).

#### Correlations between rs-fMRI BOLD signals and SjvO2

Although the ALFF values in the brains of CA patients were elevated in some brain regions and decreased in others, the mean ALFF values of the whole brain were significantly greater in CA patients than in healthy controls ($P = 0.010$). Interestingly, there was a strong correlation between the mean ALFF and SjvO2 in CA patients ($r = 0.910$, $P < 0.001$, Fig. 4C). The mean fALFF values and mean ReHo values of the whole brain had a poor correlation with SjvO2.

#### Correlations between rs-fMRI BOLD signals and SSEP responses

We analyzed the correlations between the rs-fMRI BOLD signals of the left thalamus, insula, postcentral gyrus and rolandic operculum and SSEP N20-baseline amplitude. CA patients were divided into CPC 1–2 group and CPC 3–5 group, and then CPC 3–5 group was categorized into N20 presence and absence groups. The median ALFF, fALFF and ReHo values in each group are shown in Table 3. There were no differences between healthy controls and those in the CPC 1–2 group ($P > 0.05$). However, the rs-fMRI measurements in the CPC 1–2 group showed a stepwise change compared to those in the N20 presence and absence groups. The most significant differences in the conduction pathways were the rs-fMRI BOLD signals in the thalamus (all $P < 0.001$). Correlation analysis revealed that the SSEP N20-baseline amplitudes in CA patients were negatively correlated with thalamic

**Table 2** The abnormal rs-fMRI BOLD signals clusters in localized brain regions of patients with cardiac arrest

| Region | Mni coordinate | | | Cluster size (Voxels) | Peak T value |
|---|---|---|---|---|---|
| | X | Y | Z | | |
| ALFF values | | | | | |
| *HCs > CA patients:* | | | | | |
| Left superior parietal gyrus | − 10 | − 62 | 72 | 107 | − 5.569 |
| Right superior parietal gyrus | 46 | − 52 | 58 | 280 | − 5.559 |
| *HCs < CA patients:* | | | | | |
| Right paracentral lobule, postcentral gyrus, median cingulate | 10 | − 36 | 64 | 400 | 4.940 |
| Left paracentral lobule, postcentral gyrus, median cingulate | − 12 | − 38 | 58 | 169 | 4.926 |
| White matter of right frontal, parietal and insula lobe | 44 | -26 | 34 | 379 | 5.051 |
| *CPC 1–2 group > CPC 3–5 group:* | | | | | |
| Left middle temporal gyrus, inferior temporal gyrus | − 62 | − 40 | − 16 | 330 | 6.758 |
| fALFF values | | | | | |
| *HCs > CA patients:* | | | | | |
| Right superior parietal gyrus | 48 | − 52 | 58 | 582 | -5.818 |
| Left superior parietal gyrus | − 10 | − 62 | 74 | 344 | − 5.558 |
| Bilateral occipital lobe, left cerebellum (1) | − 6 | − 92 | 38 | 825 | − 5.073 |
| Right temporal lobe | 60 | − 54 | 20 | 218 | − 5.750 |
| Reho values | | | | | |
| *HCs > CA patients:* | | | | | |
| Right frontal lobe | 26 | 4 | 68 | 225 | − 5.943 |
| Left frontal lobe | -24 | 4 | 66 | 247 | − 4.723 |
| Bilateral parietal lobe, occipital lobe, median and posterior cingulate gyrus | 12 | − 86 | 42 | 2260 | − 5.940 |
| *HCs < CA patients:* | | | | | |
| Bilateral fusiform gyrus, hippocampus, parahippocampal, insula, Cerebellum (4–5), Vermis (1–5), right putamen, and white matter of bilateral temporal lobe | 38 | − 52 | 0 | 7784 | 8.097 |
| *CPC 1–2 group > CPC 3–5 group:* | | | | | |
| Right precentral gyrus, superior frontal gyrus and middle frontal gyrus | 42 | 8 | 58 | 512 | 7.389 |
| Bilateral parietal lobe | − 4 | − 80 | 40 | 2403 | 8.275 |
| *CPC 1–2 group < CPC 3–5 group:* | | | | | |
| Left Insula | − 34 | 18 | 8 | 360 | − 5.387 |
| Left hippocampus, parahippocampal and white matter of left frontal and temporal lobe | − 26 | − 28 | 22 | 473 | − 6.703 |

ALFF Amplitude of Low Frequency Fluctuation, BOLD blood oxygenation level-dependent, CA cardiac arrest, CPC cerebral performance category, fALFF fractional Amplitude of Low Frequency Fluctuation, HC healthy controls, ReHo Regional Homogeneity, rs-fMRI Resting-state functional Magnetic Resonance Imaging

BOLD signals, including ALFF ($r = -0.777$, $P < 0.001$, Fig. 5A), fALFF ($r = -0.586$, $P = 0.001$, Fig. 5B), and ReHo ($r = -0.643$, $P < 0.001$, Fig. 5C).

## Discussion

This study focused on detecting early changes in rs-fMRI BOLD signals in comatose patients after CA. In this cohort study, we ensured the homogeneity of the enrolled patient population, including resuscitated patients with presumed cardiac causes, patients with initial shockable rhythms, patients with witnessed arrests, and the consistency in the timing of MRI examinations. The potential confounding factors that may affect BOLD signals, such as PaCO2 levels, haemoglobin levels, pH, PaO2, and hemodynamics, remained consistent. This study showed that the BOLD signals of resuscitated patients revealed complex changes, characterized by increased activity in some local brain regions and reduced activity in others compared to those of healthy controls. Abnormal BOLD signals were associated with neurological outcomes in resuscitated patients. The mean ALFF values of the whole brain were closely related to SjvO2 levels. The extent of thalamic damage as revealed by BOLD signals may determine SSEP N20-baseline amplitudes.

The pathophysiology of HIBI can be divided into primary and secondary injuries, which are caused by cerebral ischemia during CA and reperfusion after successful resuscitation. Due to the varying tolerances of different brain regions to ischemia and hypoxia, neurological damage in the brain may manifest as a mixed presentation

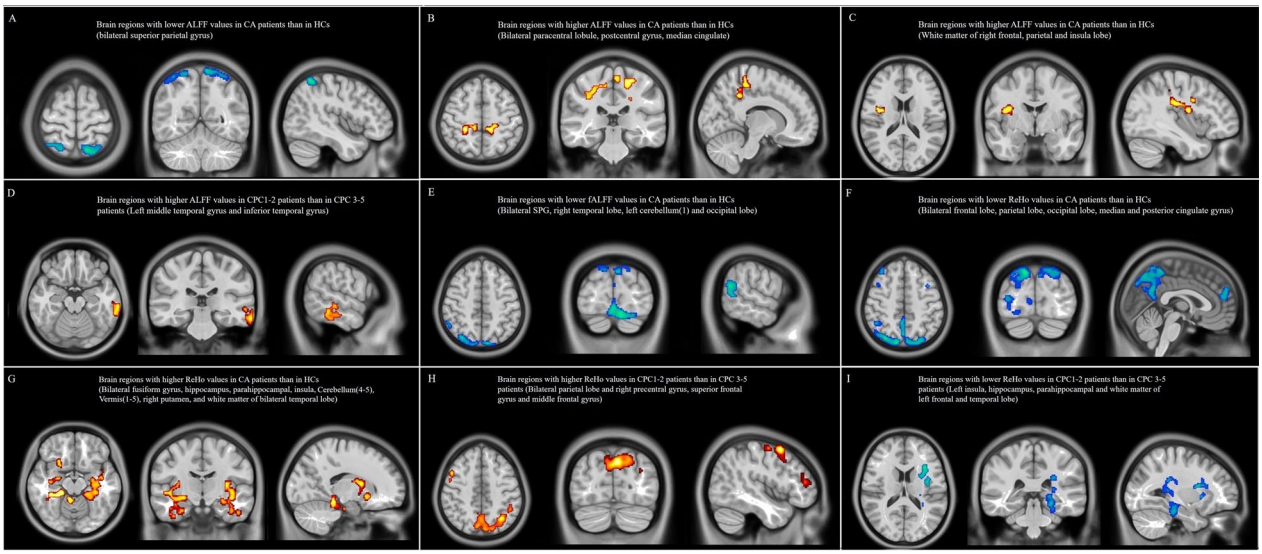


**Fig. 2** The abnormal rs-fMRI BOLD signals clusters in localized brain regions of patients with cardiac arrest. Clusters indicating regions with significant increases in activity are highlighted in red-yellow, while those with significant decreases in activity are depicted in blue-white. In comparison to the healthy controls, CA patients exhibited reduced BOLD signals primarily in the cortex, while increased BOLD signals were predominantly distributed in subcortical areas. Patients in the CPC 1–2 group showed increased BOLD signals in the cortical regions compared to those in the CPC 3–5 group

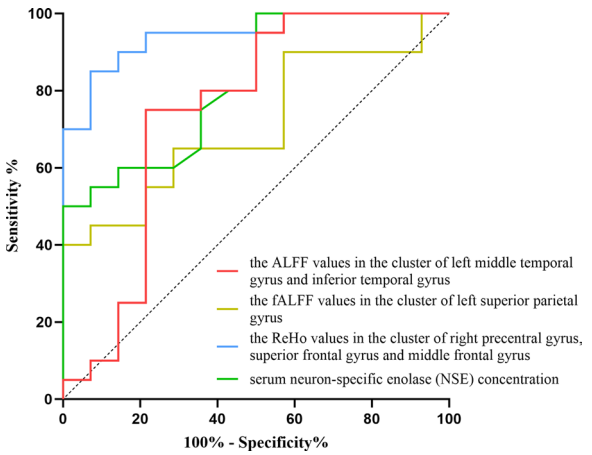


**Fig. 3** Receive operating characteristic curve for predicting poor prognosis of rs-fMRI BOLD signals and serum NSE concentration in post-resuscitated patients. Areas under the curve (AUCs) for poor prognosis: the ALFF values in the cluster of left middle temporal gyrus and inferior temporal gyrus (red line) 0.794, the fALFF values in the cluster of left superior parietal gyrus (yellow line) 0.728, the ReHo values in the cluster of right precentral gyrus, superior frontal gyrus and middle frontal gyrus (blue line) 0.943, the serum NSE concentration (green line) 0.820

where some brain regions experience no-reflow, others exhibit hypoperfusion, and still others exhibit hyperemia [3, 20]. Regional cerebral blood flow alterations result in changes in deoxyhemoglobin concentration, which are manifested by abnormal rs-fMRI BOLD signals [21]. Due to the complex changes in cerebral hemodynamics after CA, BOLD signals in different brain regions exhibit varying manifestations, characterized by increased activity in some local brain regions and reduced activity in others. The decreased BOLD signals may reflect regional dysfunction, accompanied by reduced local cerebral perfusion [22, 23]. The increased BOLD signals might reflect a compensatory mechanism of the brain to maintain a desired function [19, 24]. We found that, in comparison to healthy controls, CA patients exhibited reduced BOLD signals primarily in localized cortical areas. This finding may be attributed to the high susceptibility of the cortex to hypoxia. Patients in the CPC 1–2 group showed increased BOLD signals in cortical regions compared to those in the CPC 3–5 group. This result may suggest that patients with a favorable prognosis have better compensatory function in their cortex.

The regional biomarkers indicative of poor prognosis following OHCA are primarily identified using MRI technology. Michael and colleagues showed that cortical structures, in particular the occipital and temporal lobes, and the putamen exhibited the most profound apparent diffusion coefficient reductions in poor-outcome patients after CA [25]. These brain regions have partial overlap with our study. However, their study population includes patients with in-hospital and out-of-hospital cardiac arrests, encompassing a variety of etiologies. Previous studies have also investigated the relationship between connectivity of rs-fMRI and neurological outcomes in

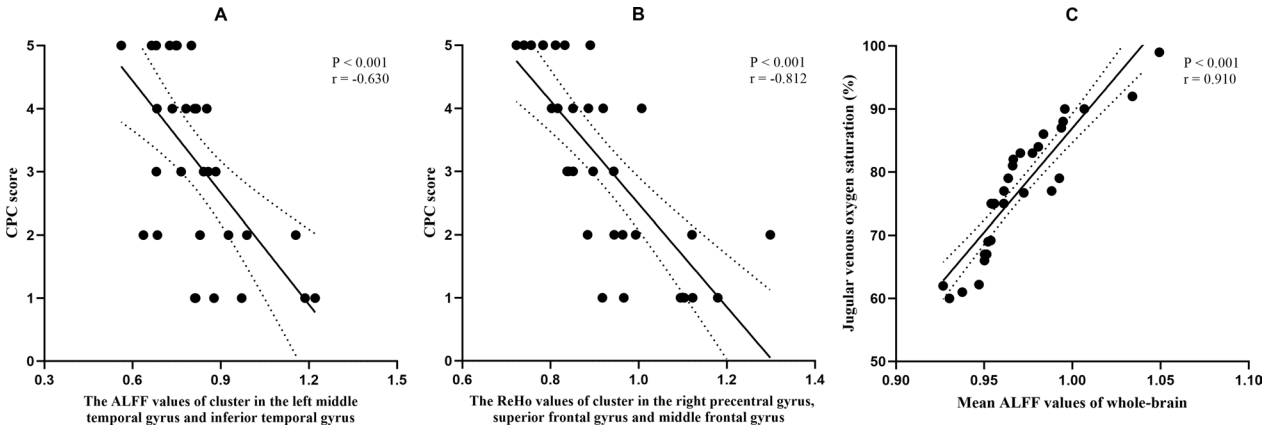


**Fig. 4** The correlation between the rs-fMRI BOLD signals and CPC score and the correlation between the mean ALFF values of whole-brain. The ALFF values of the clusters in the left middle temporal gyrus and inferior temporal gyrus showed a significant negative correlation with the CPC score (r = -0.630, $P < 0.001$). **A** The ReHo values of the clusters in the right prefrontal, superior frontal, and middle frontal gyri showed a strong negative correlation with the CPC score (r = − 0.812, $P < 0.001$). **B** The mean ALFF values of whole brain showed a strong positive correlation with SjvO2 (r = 0.910, $P < 0.001$). **C** The dashed line in the figure is the regression line with 95% confidence intervals of the slope

**Table 3** The rs-fMRI BOLD signals of localized brain regions within the intracerebral conduction pathways for SSEP

| | HCs (n = 20) | CPC 1–2 (n = 12) | CPC 3–5 (n = 19) | | *P* value |
|---|---|---|---|---|---|
| | | | N20 present (n = 11) | N20 absent (n = 8) | |
| *ALFF values* | | | | | |
| Postcentral gyrus | 0.89 (0.83–0.95) | 0.91 (0.88–0.96) | 0.84 (0.82–0.89) | 0.81 (0.77–0.85) | 0.037 |
| Rolandic operculum | 1.00 (0.96–1.06) | 1.04 (1.01–1.06) | 1.05 (0.99–1.07) | 1.03 (0.98–1.08) | 0.440 |
| Insula | 1.15 (1.05–1.21) | 1.09 (1.03–1.14) | 1.10 (1.09–1.14) | 1.11 (1.08–1.15) | 0.376 |
| Thalamus | 0.90 (0.85–0.92) | 0.90 (0.83–0.93) | 0.95 (0.88–1.07) | 1.06 (1.03–1.08) | < 0.001 |
| *fALFF values* | | | | | |
| Postcentral gyrus | 0.90 (0.88–0.92) | 0.90 (0.90–0.93) | 0.87 (0.85–0.94) | 0.86 (0.85–0.89) | 0.040 |
| Rolandic operculum | 0.95 (0.94–0.98) | 0.97 (0.96–0.99) | 0.99 (0.96–0.99) | 0.96 (0.95–0.97) | 0.200 |
| Insula | 0.99 (0.96–1.03) | 0.97 (0.95–1.01) | 1.00 (0.98–1.03) | 1.00 (0.99–1.01) | 0.099 |
| Thalamus | 0.90 (0.89–0.92) | 0.91 (0.90–0.95) | 1.00 (0.90–1.01) | 1.00 (0.98–1.01) | < 0.001 |
| *ReHo values* | | | | | |
| Postcentral gyrus | 1.01(0.93–1.07) | 1.02 (0.98–1.07) | 0.89 (0.86–1.14) | 0.88 (0.84–0.89) | 0.002 |
| Rolandic operculum | 0.87 (0.84–0.89) | 0.90 (0.88–0.92) | 0.92 (0.89–0.93) | 0.93 (0.91–0.93) | 0.009 |
| Insula | 0.85 (0.79–0.89) | 0.88 (0.82–0.92) | 0.93 (0.89–0.97) | 0.95 (0.89–0.99) | 0.001 |
| Thalamus | 0.73 (0.66–0.76) | 0.71 (0.68–0.74) | 0.81 (0.69–0.90) | 0.89 (0.83–0.94) | < 0.001 |

Data are shown as median and interquartile range unless otherwise indicated

ALFF Amplitude of Low Frequency Fluctuation, BOLD blood oxygenation level-dependent, CPC cerebral performance category, fALFF fractional Amplitude of Low Frequency Fluctuation, HCs healthy controls, ReHo Regional Homogeneity, rs-fMRI Resting-state functional Magnetic Resonance Imaging, SSEP Somatosensory evoked potentials

CA patients. Pugin and colleagues reported higher functional connectivity according to rs-fMRI in patients who were recovering consciousness (n = 17) [26]. However, their study population included patients with in-hospital and out-of-hospital cardiac arrests, and they did not clarify the consistency of various confounding factors that may affect rs-fMRI BOLD signals. Keijzer and colleagues showed that resting-state functional connectivity was strongly associated with neurological recovery (n = 48) [8]. However, only 28 patients were in a comatose state during the MRI examination, and the etiologies and confounding factors were not specified in their study. Other studies showed that patients with unfavorable outcomes typically exhibited decreased network strengths in the default mode network, with MRI examinations conducted between 4 and 13 days after CA [9, 10, 27].

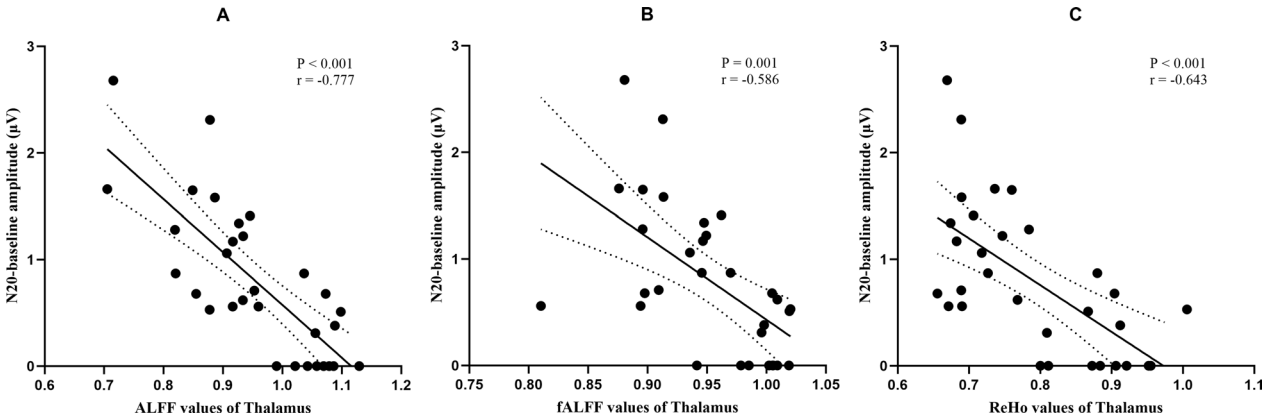


**Fig. 5** The correlation between the rs-fMRI BOLD signals of thalamus and the SSEP N20-baseline amplitudes. The SSEP N20-baseline amplitudes were negatively correlated with the thalamic BOLD signals, including the ALFF values ($r = -0.777$, $P < 0.001$), **A** the fALFF values ($r = -0.586$, $P = 0.001$), **B** and the ReHo values ($r = -0.643$, $P < 0.001$), **C** the dashed line in the figure is the regression line with 95% confidence intervals of the slope

However, most of these studies did not quantify abnormal neural activity in specific brain regions. Wu and colleagues reported that alterations in the regional neural activity of rs-fMRI BOLD signals were associated with cognitive and physical impairments in CA survivors with preserved neurological function (n = 13) [28]. However, the MRI examinations in their study were performed at 14.85 ± 4.90 days after CA when the patient was in stable condition. In this study, the study sample was as homogeneous as possible, and potential confounding factors remained consistent. Furthermore, our study demonstrated the characteristics of altered early regional neural activity observed through rs-fMRI in comatose survivors of CA.

The relationships between the rs-fMRI BOLD signals and neurological outcomes were also evaluated in resuscitated patients. ALFF showed decreased activity in the cluster of the left middle temporal gyrus and inferior temporal gyrus in the CPC 3–5 group compared to the CPC 1–2 group. The activity of this cluster was associated with favorable prognosis in patients after CA. The middle temporal gyrus and inferior temporal gyrus are involved in several cognitive processes [29, 30]. The decreased ALFF values of these regions may suggest potential cognitive impairments in resuscitated patients. ReHo exhibited a broader distribution of abnormal regions in the CPC 3–5 group. Of these, the clusters of the right anterior frontal gyrus, superior frontal gyrus, and middle frontal gyrus were more strongly associated with poor functional recovery. Interestingly, these regions are involved in conscious perception, attention and memory and executive functions [31, 32]. Our investigation also revealed significant differences in ReHo values within specific brain regions, including the parietal lobe, the left hippocampus, the parahippocampal region, and the white matter of the left frontal and temporal lobes. The parietal lobe may be involved in integrating information from different sensory modalities, contributing to conscious awareness [33]. The left insula plays a significant role in the formation and regulation of consciousness, particularly in emotional awareness and self-awareness [34]. The left hippocampus is implicated in the integration of memory and the perception of time, aiding in the formation of a continuous sense of self [35]. The parahippocampal area is particularly involved in visual memory and scene recognition [36]. The white matter of the left frontal and temporal lobes may facilitate rapid information exchange between different brain regions, which is crucial for the formation of a coherent conscious experience [37]. Notably, the predictive potential of the ReHo was greater than that of the serum NSE concentration in resuscitated patients. The possible reason for this may be that rs-fMRI BOLD signals can be direct indicators of changes in local brain activity, whereas the serum NSE concentration is an indirect indicator based on its release into the peripheral blood through the compromised blood brain barrier (BBB) [38].

Another interesting finding of this study was that the mean ALFF values of the whole brain were closely related to SjvO2 levels. An increased mean SjvO2 was often associated with unfavorable outcomes in patients after CA [12, 13]. Impaired oxygen diffusion or compensatory mechanisms for hypoxic-ischemic brain injury result in elevated levels of oxyhemoglobin and reduced levels of deoxyhemoglobin in cerebral capillaries, as evidenced by increased ALFF values. This phenomenon may lead to the "arterialization" of venous blood, which manifests as elevated SjvO2 levels.

The SSEP is one of the guideline-recommended multimodal prediction approaches for assessing the initiation of withdrawal of life-sustaining treatment (WLST) [4, 39]. The bilateral absence of N20 SSEP responses is considered a reliable predictor of poor prognosis, however its sensitivity is only approximately 30% [4, 40]. Some studies have suggested that a low N20-baseline amplitude may have a higher sensitivity for predicting poor outcomes in resuscitated patients [16, 17]. These alterations may depend on the extent of damage to the thalamocortical loop, particularly involving the thalamus. This study demonstrated that the N20-baseline amplitudes were strongly correlated with the degree of thalamic damage, as reflected in the rs-fMRI BOLD signal. Interestingly, postmortem histopathology in postanoxic coma patients revealed that the absence of SSEP responses was always accompanied by thalamic damage [15]. Notably, previous studies have shown that a high N20-baseline amplitude predicts a good prognosis with high specificity but low to moderate sensitivity [16, 41]. The pathophysiological mechanism of this phenomenon may be elucidated in our research. Although the intracerebral conduction pathways for SSEP remain intact, abnormal activity in other localized brain regions associated with conscious perception and processing may also lead to unfavorable neurological prognosis.

This study has several limitations. First, the study population included patients with CA that was considered cardiac cause, an initial shockable rhythm and witnessed arrests. The different etiologies of CA may involve in different pathophysiological mechanism [42, 43]. And other variables, such as the quality of CPR and time to ROSC, may affect the degree of cerebral hypoxia–ischemia in patients with CA. Therefore, it is important to note that the abnormal rs-fMRI BOLD signals observed in this study may not be generalizable to all patients with CA. And despite our efforts to control for the impact of potential confounding factors, the influence of respiratory variations during the MRI examination may not be entirely eliminated. Second, the impaired oxygen diffusion or compensatory mechanisms in HIBI may undergo changes over time. Dynamic monitoring of rs-fMRI BOLD signals in resuscitated patients may provide additional valuable information. Studies have demonstrated that breath-hold challenges can serve as a useful tool to probe cerebrovascular reactivity, which was mapped using the BOLD signal of fMRI [44, 45]. Incorporating breath-hold paradigms into rs-fMRI protocols to directly assess cerebrovascular reactivity in resuscitated patients may provide additional information regarding neurological prognosis. Third, quantitative electroencephalography (qEEG) was not included in the study. qEEG analyses the electrical activity of the brain to measure and display patterns that correspond to diagnostic information [46]. Investigating the correlation between qEEG and rs-fMRI BOLD signals could be an interesting direction for future research. Fourth, this study focused on the local function of specific brain regions through the analysis of rs-fMRI activity. The functional connectivity between different brain areas could be detected using rs-fMRI connectivity analysis [47]. Examining both the local and global organization of brain networks in resuscitated patients may reveal more comprehensive information.

## Conclusions

This study revealed that abnormal rs-fMRI BOLD signals in resuscitated patients showed complex changes, characterized by increased activity in some local brain regions and reduced activity in others. Abnormal BOLD signals were associated with neurological outcomes in resuscitated patients. The mean ALFF values of the whole brain were closely related to SjvO2 levels, and changes in thalamic BOLD signals correlated with the N20-baseline amplitudes of SSEP responses.

### Abbreviations

| | |
|---|---|
| ABG | Arterial blood gas |
| ALFF | Amplitude of low frequency fluctuation |
| AUC | Area under the curve |
| BBB | Blood–brain barrier |
| BOLD | Blood oxygenation level-dependent |
| CA | Cardiac arrest |
| CPC | Cerebral performance category |
| CPR | Cardiopulmonary resuscitation |
| DMN | Default-mode network |
| EICU | Emergency intensive care unit |
| fALFF | Fractional ALFF |
| HIBI | Hypoxic ischemic brain injury |
| IQR | Interquartile spacing |
| NSE | Neuron specific enolase |
| OHCA | Out-of-hospital cardiac arrest |
| PaCO2 | Partial pressure of carbon dioxide in arterial blood |
| PaO2 | Partial pressure of oxygen in arterial blood |
| PbtO2 | Brain tissue oxygen tension |
| PvO2 | Cerebral venous partial pressure of oxygen |
| qEEG | Quantitative electroencephalography |
| RASS | Richmond agitation–sedation scale |
| ReHo | Regional homogeneity |
| rs-fMRI | Resting-state functional magnetic resonance imaging |
| ROC | Receiver operating characteristic |
| ROSC | Return of spontaneous circulation |
| SjvO2 | Jugular venous oxygen saturation |
| SSEP | Somatosensory evoked potential |
| WLST | Withdrawal of life-sustaining treatment |

## Supplementary Information

The online version contains supplementary material available at https://doi.org/10.1186/s13054-024-05045-4.

Additional file 1.

Additional file 2.

**Acknowledgements**
The study was conducted thanks to the helpful contributions of the Department of Radiology staff.

**Author contributions**
Shao R and Wang T contributed to study conception and writing. Wang X, Zhang L, Yu J and Shan Z contributed to data acquisition. Hang C and An L contributed to statistical analysis and revision. Yang Q contributed to imaging data analysis and result interpretation. Tang Z contributed to study design and acquisition of funding.

**Funding**
High-Level Public Health Technical Talent Building Program (Discipline Leader-01-01), Capital's Funds for Health Improvement and Research (CFH 2022-1-2032), National Natural Science Foundation of China (82072136, 82025030), Beijing Hospitals Authority's Ascent Plan (DFL20240302).

**Availability of data and materials**
The datasets used and/or analysed during the current study are available from the corresponding author on reasonable request.

## Declarations

**Ethics approval and consent to participate**
The study was conducted according to the guidelines of the Declaration of Helsinki and approved by the Institutional Review Board of Beijing Chao-yang Hospital (No. 2023-ke-406). Informed consent (participation and publication) was obtained from all patients and/or legal surrogate.

**Consent for publication**
Not applicable.

**Competing interests**
The authors declare no competing interests.

**Author details**
[1]Department of Emergency Medicine, Beijing Chaoyang Hospital, Capital Medical University, 8# Worker's Stadium South Road, Chao-yang District, Beijing 100020, China. [2]Department of Radiology, Beijing Chaoyang Hospital, Capital Medical University, 8# Worker's Stadium South Road, Chao-yang District, Beijing 100020, China.

Received: 9 May 2024 Accepted: 21 July 2024
Published online: 02 August 2024

**References**

1. Geocadin RG, Callaway CW, Fink EL, et al. Standards for studies of neurological prognostication in comatose survivors of cardiac arrest: a scientific statement from the American heart association. Circulation. 2019;140(9):e517–42.
2. Sandroni C, Cronberg T, Sekhon M. Brain injury after cardiac arrest: pathophysiology, treatment, and prognosis. Intensive Care Med. 2021;47(12):1393–414.
3. Sekhon MS, Ainslie PN, Griesdale DE. Clinical pathophysiology of hypoxic ischemic brain injury after cardiac arrest: a "two-hit" model. Crit Care. 2017;21(1):90.
4. Nolan JP, Sandroni C, Böttiger BW, et al. European resuscitation council and European society of intensive care medicine guidelines 2021: post-resuscitation care. Intensive Care Med. 2021;47(4):369–421.
5. Moseby-Knappe M, Westhall E, Backman S, et al. Performance of a guideline-recommended algorithm for prognostication of poor neurological outcome after cardiac arrest. Intensive Care Med. 2020;46(10):1852–62.
6. Bongiovanni F, Romagnosi F, Barbella G, et al. Standardized EEG analysis to reduce the uncertainty of outcome prognostication after cardiac arrest. Intensive Care Med. 2020;46(5):963–72.
7. Lv H, Wang Z, Tong E, et al. Resting-state functional MRI: everything that nonexperts have always wanted to know. AJNR Am J Neuroradiol. 2018;39(8):1390–9.
8. Keijzer HM, Lange PAM, Meijer FJA, et al. MRI markers of brain network integrity relate to neurological outcome in postanoxic coma. Neuroimage Clin. 2022;36:103171.
9. Sair HI, Hannawi Y, Li S, et al. Early functional connectome integrity and 1-year recovery in comatose survivors of cardiac arrest. Radiology. 2018;287(1):247–55.
10. Koenig MA, Holt JL, Ernst T, et al. MRI default mode network connectivity is associated with functional outcome after cardiopulmonary arrest. Neurocrit Care. 2014;20(3):348–57.
11. Macmillan CS, Andrews PJ. Cerebrovenous oxygen saturation monitoring: practical considerations and clinical relevance. Intensive Care Med. 2000;26(8):1028–36.
12. Richter J, Sklienka P, Chatterjee N, et al. Elevated jugular venous oxygen saturation after cardiac arrest. Resuscitation. 2021;169:214–9.
13. Hoedemaekers CW, Ainslie PN, Hinssen S, et al. Low cerebral blood flow after cardiac arrest is not associated with anaerobic cerebral metabolism. Resuscitation. 2017;120:45–50.
14. Ferretti A, Babiloni C, Arienzo D, et al. Cortical brain responses during passive nonpainful median nerve stimulation at low frequencies (0.5–4 Hz): an fMRI study. Hum Brain Mapp. 2007;28(7):645–53.
15. van Putten M, Jansen C, Tjepkema-Cloostermans MC, et al. Postmortem histopathology of electroencephalography and evoked potentials in postanoxic coma. Resuscitation. 2019;134:26–32.
16. Benghanem S, Nguyen LS, Gavaret M, et al. SSEP N20 and P25 amplitudes predict poor and good neurologic outcomes after cardiac arrest. Ann Intensive Care. 2022;12(1):25.
17. Scarpino M, Lolli F, Lanzo G, et al. SSEP amplitude accurately predicts both good and poor neurological outcome early after cardiac arrest; a post-hoc analysis of the ProNeCA multicentre study. Resuscitation. 2021;163:162–71.
18. Wang R, Liu X, Sun C, et al. Altered neurovascular coupling in patients with mitochondrial myopathy, encephalopathy, lactic acidosis, and stroke-like episodes (MELAS): a combined resting-state fMRI and arterial spin labeling study. J Magn Reson Imaging. 2024;60(1):327–36.
19. Wang L, Wang S, Zheng W, et al. Altered brain function in pediatric patients with complete spinal cord injury: a resting-state functional MRI study. J Magn Reson Imaging. 2023;60:304–13.
20. Schoenthal T, Hoiland R, Griesdale DE, et al. Cerebral hemodynamics after cardiac arrest: implications for clinical management. Minerva Anestesiol. 2023;89(9):824–33.
21. Toronov V, Walker S, Gupta R, et al. The roles of changes in deoxyhemoglobin concentration and regional cerebral blood volume in the fMRI BOLD signal. Neuroimage. 2003;19(4):1521–31.
22. Ovadia-Caro S, Margulies DS, Villringer A. The value of resting-state functional magnetic resonance imaging in stroke. Stroke. 2014;45(9):2818–24.
23. Chen Q, Zhou J, Zhang H, et al. One-step analysis of brain perfusion and function for acute stroke patients after reperfusion: a resting-state fMRI study. J Magn Reson Imaging. 2019;50(1):221–9.
24. Mohammadi B, Kollewe K, Samii A, et al. Functional neuroimaging at different disease stages reveals distinct phases of neuroplastic changes in amyotrophic lateral sclerosis. Hum Brain Mapp. 2011;32(5):750–8.
25. Mlynash M, Campbell DM, Leproust EM, et al. Temporal and spatial profile of brain diffusion-weighted MRI after cardiac arrest. Stroke. 2010;41(8):1665–72.
26. Pugin D, Hofmeister J, Gasche Y, et al. Resting-state brain activity for early prediction outcome in postanoxic patients in a coma with indeterminate clinical prognosis. AJNR Am J Neuroradiol. 2020;41(6):1022–30.
27. Norton L, Hutchison RM, Young GB, et al. Disruptions of functional connectivity in the default mode network of comatose patients. Neurology. 2012;78(3):175–81.
28. Wu Q, Wang GN, Hu H, et al. A resting-state functional magnetic resonance imaging study of altered functional brain activity in cardiac arrest survivors with good neurological outcome. Front Neurol. 2023;14:1136197.
29. Cabeza R, Nyberg L. Imaging cognition II: an empirical review of 275 PET and fMRI studies. J Cogn Neurosci. 2000;12(1):1–47.
30. Mesulam MM. From sensation to cognition. Brain. 1998;121(Pt 6):1013–52.

31. Naber M, Brascamp J. Commentary: is the frontal lobe involved in conscious perception? Front Psychol. 2015;6:1736.
32. Friedman NP, Robbins TW. The role of prefrontal cortex in cognitive control and executive function. Neuropsychopharmacology. 2022;47(1):72–89.
33. Fogassi L, Ferrari PF, Gesierich B, et al. Parietal lobe: from action organization to intention understanding. Science. 2005;308(5722):662–7.
34. Craig AD. How do you feel–now? The anterior insula and human awareness. Nat Rev Neurosci. 2009;10(1):59–70.
35. Sherman BE, DuBrow S, Winawer J, et al. Mnemonic content and hippocampal patterns shape judgments of time. Psychol Sci. 2023;34(2):221–37.
36. Aminoff EM, Kveraga K, Bar M. The role of the parahippocampal cortex in cognition. Trends Cogn Sci. 2013;17(8):379–90.
37. Li X, Jiang Y, Li W, et al. Disrupted functional connectivity in white matter resting-state networks in unilateral temporal lobe epilepsy. Brain Imaging Behav. 2022;16(1):324–35.
38. Kadry H, Noorani B, Cucullo L. A blood-brain barrier overview on structure, function, impairment, and biomarkers of integrity. Fluids Barriers CNS. 2020;17(1):69.
39. Soar J, Maconochie I, Wyckoff MH, et al. 2019 international consensus on cardiopulmonary resuscitation and emergency cardiovascular care science with treatment recommendations: summary from the basic life support; advanced life support; pediatric life support; neonatal life support; education, implementation, and teams; and first aid task forces. Circulation. 2019;140(24):e826–80.
40. van Putten MJ. The N20 in post-anoxic coma: are you listening? Clin Neurophysiol. 2012;123(7):1460–4.
41. Barbella G, Novy J, Marques-Vidal P, et al. Added value of somato-sensory evoked potentials amplitude for prognostication after cardiac arrest. Resuscitation. 2020;149:17–23.
42. Chen N, Callaway CW, Guyette FX, et al. Arrest etiology among patients resuscitated from cardiac arrest. Resuscitation. 2018;130:33–40.
43. Shaeri S, Considine J, Dainty KN, et al. Accuracy of etiological classification of out- of-hospital cardiac arrest: a scoping review. Resuscitation. 2024;198:110199.
44. Moia S, Termenon M, Uruñuela E, et al. ICA-based denoising strategies in breath-hold induced cerebrovascular reactivity mapping with multi echo BOLD fMRI. Neuroimage. 2021;233:117914.
45. Zvolanek KM, Moia S, Dean JN, et al. Comparing end-tidal CO(2), respiration volume per time (RVT), and average gray matter signal for mapping cerebrovascular reactivity amplitude and delay with breath-hold task BOLD fMRI. Neuroimage. 2023;272:120038.
46. Bauerschmidt A, Eliseyev A, Doyle KW, et al. Predicting early recovery of consciousness after cardiac arrest supported by quantitative electroencephalography. Resuscitation. 2021;165:130–7.
47. Tomasi D, Volkow ND. Functional connectivity density mapping. Proc Natl Acad Sci USA. 2010;107(21):9885–90.


## Publisher's Note